Applied Catalysis B: Environmental 191 (2016) 53–61

Contents lists available at ScienceDirect

Applied Catalysis B: Environmental

journal homepage: www.elsevier.com/locate/apcatb

Elimination of 1,2-dichloroethane over $(Ce,Cr)_xO_2/MO_y$ catalysts (M = Ti, V, Nb, Mo, W and La)

Peng Yang[a], Shufeng Zuo[b], Zhinan Shi[a], Fei Tao[a], Renxian Zhou[a,*]

[a] Institute of Catalysis, Zhejiang University, Hangzhou 310028, PR China
[b] Zhejiang Key Laboratory of Alternative Technologies for Fine Chemicals Process, Shaoxing University, Shaoxing 312000, PR China

ARTICLE INFO

Article history:
Received 9 December 2015
Received in revised form 2 March 2016
Accepted 9 March 2016
Available online 14 March 2016

Keywords:
Total oxidation
Chlorinated VOCs
Durability
Mixed oxide
Promoted effect

ABSTRACT

$(Ce,Cr)_xO_2/MO_y$ (M = Ti, V, Nb, Mo, W, La, respectively) mixed oxides are synthesized by deposition-precipitation method, and evaluated for total oxidation of gaseous 1,2-dichloroethane, a typical chlorinated organic pollutant. The characterization results show that there exists strong metal-support interaction or synergistic effect between $(Ce,Cr)_xO_2$ and MO_y. The catalytic performances of these catalysts can be related to the nature of each MO_y support, the crystal structure and composition, the surface elements distribution and the diverse redox properties of $(Ce,Cr)_xO_2/MO_y$. The improved redox property, as well as the increased content of Ce^{3+} and Cr^{6+} species on the surface can enhance the catalytic performances of the catalysts. Especially, $(Ce,Cr)_xO_2/Nb_2O_5$ exhibits the best catalytic performance. $(Ce,Cr)_xO_2/Nb_2O_5$ also represents high durability for 1,2-dichloroethane oxidation during the long-term continuous test. Moreover, though the presence of water or benzene in the reaction system slightly suppresses 1,2-dichloroethane oxidation, the catalytic activity can be recovered by the cut of water, while a little deactivation is found if benzene is removed away, since coke has been deposited on the catalyst surface by the combustion of benzene.

© 2016 Elsevier B.V. All rights reserved.

1. Introduction

Chlorinated volatile organic compounds (Cl-VOCs) contain a significant class of synthetic intermediates and organic solvents widely used in industrial operations, and are usually discharged into the environment with low concentration and large volume [1–3]. These chlorinated compounds are always toxic to human beings, and they also tend to be accumulated in the atmosphere [1,4]. Catalytic oxidation (or deep oxidation) is one of the most widely adopted methods to eliminate various kinds of Cl-VOCs with low concentration (100–10,000 ppmv), mainly due to its larger treatment capacity and lower reaction temperatures (less than 500 °C) to avoid the formation of NO_x and polychlorinated byproducts [4–6].

The main catalysts studied for Cl-VOCs elimination are supported noble metal materials, zeolites and modified zeolites, perovskites and metal oxides. Previous literatures have shown that supported noble metal catalysts generally exhibits higher catalytic activities than others, but they are more expensive and easily deactivated because of Cl poisoning and the formation of metal oxychloride, resulting in the volatilization of active species and the formation of polychlorinated byproducts [4,7,8]. Though H-type zeolites and modified zeolites display noticeable catalytic activities [3,8–11], large amount of chlorinated byproducts and CO are detected in the oxidation process, and obvious deactivation caused by coke formation is also observed because of their strong acidity and poor oxidizing ability. Perovskite catalysts with high structure stability are also widely explored, but they are less active and always need higher reaction temperatures [12]. Therefore, metal oxide catalysts (such as V_2O_5, Cr_2O_3 and MnO_2 [4]) especially CeO_2 based mixed oxides (such as CeO_2-MnO_x [13], CeO_2-ZrO_2 [14] and $Ce_xPr_{1-x}O_2$ [15]) have also been extensively investigated, and in fact they exhibit considerable oxidative activities and suitable chemical resistance to Cl-poisoning. Among them, $(Ce,Cr)_xO_2$ mixed oxide with higher oxidizing ability and structure stability shows preferable catalytic performances for total oxidation of Cl-VOCs with different molecule structures [16–19], and the atom ratio of Ce/Cr in the range of 4:1 to 2:1 is the best [19]. However, to further improve the catalytic performance, both the acid and oxidative properties need to be improved, since acid center is needed to firstly break the C—Cl bond with lower bonding energy, and the oxidative center is required next for the destruction of C—C, C—H or C=O bond. Besides, it is also necessary to introduce third component as promoter to increase the selectivity to HCl rather than Cl_2, in

* Corresponding author.
E-mail address: zhourenxian@zju.edu.cn (R. Zhou).

http://dx.doi.org/10.1016/j.apcatb.2016.03.017
0926-3373/© 2016 Elsevier B.V. All rights reserved.

order to reduce the toxicity of the final products, the deposition of Cl species and the formation of chlorinated byproducts on the surface of the catalysts. Previous literature has revealed that the addition of H-type zeolites can increase the acid property of $(Ce,Cr)_xO_2$ and thus significantly improve the catalytic activity and HCl selectivity [20], but obvious deactivation is detected due to coke formation, since there is still lack of enough oxidative sites. Therefore, the introduction of high-valence metal ions with the combination of acid and oxidative properties is promising.

The scope of this work is to systematically investigate the structure-activity relationship for 1,2-dichloroethane (DCE) oxidation over a series of $(Ce,Cr)_xO_2/MO_y$ mixed oxides (M = Ti, V, Nb, Mo, W and La, respectively). It concentrations on investigating the effect of the inherent nature of each metal oxide support, the strong metal-support interaction (SMSI) as well as the acid and redox properties of the materials on the catalytic activity, selectivity and durability for the elimination of DCE, a typical chlorinated organic pollutant. Moreover, the influence of water vapor or non-chlorinated VOCs in the reaction system on the destructive efficiency of the catalysts, is further explored, in order to simulate the real conditions for industrial application.

2. Experimental method

2.1. Catalyst preparation

The supports MO_y (M = Ti, V, Nb, Mo, W and La, respectively) were purchased from Guoyao company and further calcined in air (500 °C, 2 h), followed by mechanical milling for 0.5 h.

$(Ce,Cr)_xO_2/MO_y$ (mass ratio of $(Ce,Cr)_xO_2$ to MO_y was 1:1) were prepared by traditional deposition-precipitation method. Firstly, a certain amount of MO_y was added into the mixed solution of quantified $Ce(NO_3)_3$ and $Cr(NO_3)_3$ (atom molar ratio of Ce/Cr was 4:1), and then ultrasonic concussion for 1 h. Afterwards, 0.50 mol L^{-1} $(NH_4)_2CO_3$ was added dropwise into the above solution under vigorous stirring, and the final pH of the solution reached 9.0. Upon aged at 25 °C for 12 h, the precipitated solids were filtered, washed by distilled water and then dried in ethanol under super critical condition (265 °C, 2 h, 7.5 Mpa). The solids were subsequently calcined in air at 500 °C for 2 h. The obtained samples were named as $(Ce,Cr)_xO_2/MO_y$, and the content of Ce and Cr was 36.6%wt and 3.4%wt, respectively. For comparison, CeO_2/Nb_2O_5 and CrO_x/Nb_2O_5 were synthesized, and the content for Ce or Cr is 40.0%wt. $(Ce,Cr)_xO_2$ mixed oxide was also prepared following a similar procedure, and the contents of Ce and Cr are double than those for $(Ce,Cr)_xO_2/MO_y$.

All the samples were finally pressed into pellets and sieved to 40–60 mesh (0.3–0.45 mm) before used.

2.2. Catalyst characterization

The X-ray diffraction (XRD), UV-Raman spectroscopy, N_2 adsorption-desorption, scanning electron microscopy (SEM) and H_2 temperature-programmed reduction (H_2-TPR) characterizations were described in previous reference [18]. NH_3 temperature-programmed desorption (NH_3-TPD) experiment was given in [20] and 0.2 g sample was used each time in this work. The X-ray photoelectron spectroscopy (XPS) patterns of the materials were collected on the Thermo K-Alpha using Al-Kα radiation at 1486.6 eV/12.5 Kv, and all the spectra were calibrated based on the binding energy of C_{1s} (284.6 eV). The deconvolution of the peaks in XPS profiles was carried out using the CasaXPS software, in which the curve fitting was performed using the Gaussian–Lorentzian peak shape and Shirley type background subtraction.

2.3. Evaluation of catalytic performances

The catalytic performances of the catalysts were measured in a traditional quartz fixed-bed reactor (6 mm i.d.), and 500 mg catalyst (0.3–0.45 mm) was used each time. The reaction feed consisted of ~1000 ppmv DCE using dry air as the balance gas, and GHSV = 9,000 mL g_{cat}^{-1} h^{-1} with a total flow of 75 mL min^{-1}. The concentration of the reactant, the byproducts and the final products CO_x in the outlet of the gas flow was analyzed on-line at given temperatures by GC equipped with TCD and FID detectors. Selectivity to HCl and Cl_2 was also measured by the method mentioned in previous reference [16]. In order to further investigate the mixture effect, additional ~1000 ppmv benzene or 2.3% water vapor was injected into the reaction system. The durability of the catalysts for total oxidation of DCE was evaluated under the same condition.

3. Results and discussion

3.1. Results of catalytic performance evaluation

3.1.1. Catalytic performances for DCE destruction

Previous experiments have shown that mass transfer limitation is absent under this test condition, and no obvious DCE conversion is observed below 420 °C in blank test. Fig. 1(A) and (B) demonstrate the catalytic activities of pure $(Ce,Cr)_xO_2$, pure MO_y and $(Ce,Cr)_xO_2/MO_y$ catalysts for total oxidation of DCE. As shown in Fig. 1(A), pure MO_y and $(Ce,Cr)_xO_2$ represent diverse catalytic activities. Based on the values of $T_{50\%}$ (temperature at which the conversion of the reactant reaches 50%), the apparent catalytic activity decreases in the order of $(Ce,Cr)_xO_2$ (225 °C) ≻ TiO_2 (243 °C) ≻ La_2O_3 (296 °C) ≻ Nb_2O_5 (304 °C) ≻ ≻ V_2O_5 (438 °C) ≻ WO_3 ≻ MoO_3, which can be related to the inherent nature of each metal oxide. Interestingly, for the $(Ce,Cr)_xO_2/MO_y$ catalysts, the apparent catalytic activities are improved at different levels based on the values of $T_{50\%}$, in the order of $(Ce,Cr)_xO_2/Nb_2O_5$ (237 °C) ≻ $(Ce,Cr)_xO_2/TiO_2$ (245 °C) ≻ $(Ce,Cr)_xO_2/WO_3$ (254 °C) ≻ $(Ce,Cr)_xO_2/MoO_3$ (264 °C) ≻ $(Ce,Cr)_xO_2/La_2O_3$ (268 °C) ≻ ≻ $(Ce,Cr)_xO_2/V_2O_5$ (418 °C), implying that there exists synergistic effect between $(Ce,Cr)_xO_2$ and MO_y. For comparison, the catalytic activities of CeO_2/Nb_2O_5 and CrO_x/Nb_2O_5 are also evaluated, and the details are shown in Fig. SM1 in the Supplementary Material. As shown in Fig. SM1, $(Ce,Cr)_xO_2/Nb_2O_5$ represents higher activity than CeO_2/Nb_2O_5 or CrO_x/Nb_2O_5, indicating that there also exists synergy between CeO_2 and CrO_x, which is beneficial for DCE oxidation. Moreover, the TOF values for DCE oxidation over these catalysts are also calculated, since the values for the specific surface area of these catalysts are different (shown in Table 1) and obvious thermal effect may exist at higher DCE conversion. As listed in Table 1, the TOF values decrease in the order of $(Ce,Cr)_xO_2/Nb_2O_5$ ≻ $(Ce,Cr)_xO_2/WO_3$ ≻ $(Ce,Cr)_xO_2/TiO_2$ ≻ $(Ce,Cr)_xO_2/V_2O_5$ ≻ $(Ce,Cr)_xO_2$ ≻ $(Ce,Cr)_xO_2/La_2O_3$ ≻ $(Ce,Cr)_xO_2/MoO_3$, indicating that $(Ce,Cr)_xO_2/Nb_2O_5$ represents the highest inherent catalytic activity. Besides, the values of apparent activation energy (Ea) for these catalysts are also calculated, assuming DCE concentration having no obvious change within 20% conversion. As listed in Table 1, Ea values for $(Ce,Cr)_xO_2/MO_y$ are in the range of 35–47 kJ/mol, similar to or even smaller than that of $(Ce,Cr)_xO_2$. It is notable that these values are much smaller than those for the related support MO_y, further implying that there exists synergistic effect between $(Ce,Cr)_xO_2$ and MO_y.

For catalytic elimination of Cl-VOCs, any possible byproducts should be detected carefully, since they may be more toxic and more difficult to be destroyed. As shown in Fig. 1(C) and (D), within the detection limit of TCD and FID detector, C_2H_3Cl is the sole byproduct detected during DCE oxidation,

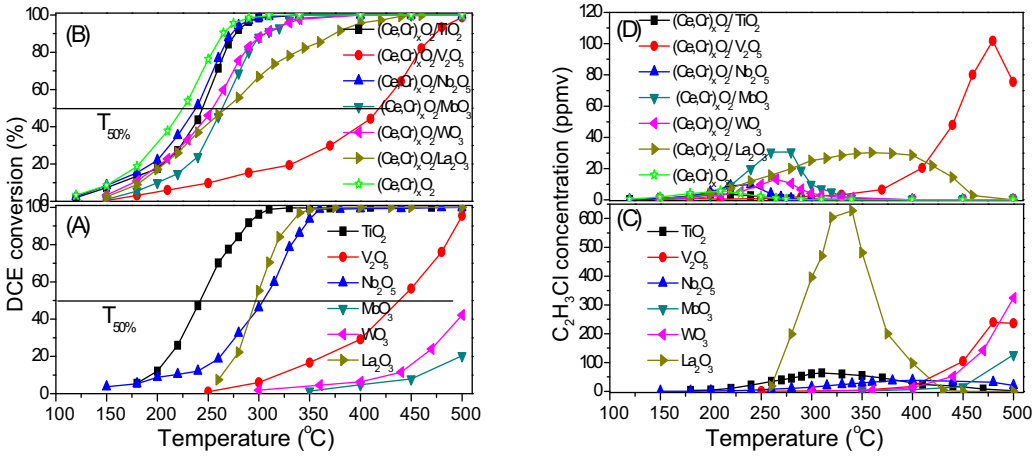

Fig. 1. Results of catalytic performance test for DCE oxidation over different catalysts: (A) and (B) DCE conversion; (C) and (D) concentration of byproduct C_2H_3Cl detected in the oxidation process.

Table 1
Related data for the catalysts studied.

Catalyst	S_{BET}/ (m^2/g)	TOF[a]/(10^{-7} mol_{DCE} m^{-2} h^{-1})	E_a/(KJ mol^{-1})	S_{HCl}[b]/(%)	Strong acid/(μmol NH_3/m^2)	Total acid/(μmol NH_3/m^2)
$(Ce,Cr)_xO_2/TiO_2$	60.3 (44.8)[c]	4.66	34.8 (69.1)[c]	89.4 (94.6)[c]	1.80	1.98
$(Ce,Cr)_xO_2/V_2O_5$	12.3 (11.9)[c]	4.58	35.7 (49.6)[c]	70.5 (93.4)[c]	4.19	5.70
$(Ce,Cr)_xO_2/Nb_2O_5$	60.9 (44.3)[c]	5.05	36.1 (37.3)[c]	82.6 (99.4)[c]	1.83	2.15
$(Ce,Cr)_xO_2/MoO_3$	41.4 (2.1)[c]	2.64	46.8 (69.5)[c]	93.1 (98.2)[c]	2.14	3.20
$(Ce,Cr)_xO_2/WO_3$	25.7 (18.0)[c]	4.79	43.6 (65.8)[c]	86.4 (98.6)[c]	1.50	3.19
$(Ce,Cr)_xO_2/La_2O_3$	44.4 (19.5)[c]	4.06	41.1 (47.4)[c]	99.4 (98.2)[c]	0.191	0.352
$(Ce,Cr)_xO_2$	82.8	4.51	42.5	59.9	1.14	1.52

[a] Measured at 180 °C.
[b] $S_{HCl} = [HCl]/([HCl] + 2[Cl_2])$; selectivity to HCl and CO_2 is measured at 360 °C, while for V_2O_5, MoO_3, WO_3, La_2O_3, $(Ce,Cr)_xO_2/V_2O_5$ and $(Ce,Cr)_xO_2/La_2O_3$, the reaction temperature is 500 °C.
[c] Data for the related support.

and any other possible byproducts (such as phosgene, chloroform, CCl_4 and dioxins) are not detected over these investigated catalysts. As to MO_y, noticeable C_2H_3Cl is detected, except for Nb_2O_5, over which the maximum concentration is only 38 ppmv appearing at lower temperature. For the $(Ce,Cr)_xO_2/MO_y$ catalysts, C_2H_3Cl concentration decreases obviously than those over MO_y, since $(Ce,Cr)_xO_2$ displays high oxidizing ability. The sequence for the maximum concentration is as follows: $(Ce,Cr)_xO_2/TiO_2$ (4 ppmv, 200 °C) ≺ $(Ce,Cr)_xO_2$ (6 ppmv, 210 °C) ≺ $(Ce,Cr)_xO_2/Nb_2O_5$ (10 ppmv, 240 °C) ≺ $(Ce,Cr)_xO_2/WO_3$ (13 ppmv, 265 °C) ≺ $(Ce,Cr)_xO_2/MoO_3$ (31 ppmv, 280 °C), $(Ce,Cr)_xO_2/La_2O_3$ (31 ppmv, 360 °C) ≺≺ $(Ce,Cr)_xO_2/V_2O_5$ (102 ppmv, 480 °C), which can be related to the different redox and surface acid properties of these catalysts. Besides, as shown in Fig. SM1, compared to CeO_2/Nb_2O_5 or CrO_x/Nb_2O_5, less concentration of C_2H_3Cl is detected over $(Ce,Cr)_xO_2/Nb_2O_5$, indicating that the synergy between CeO_2 and CrO_x is beneficial for C_2H_3Cl oxidation.

For total oxidation of DCE, the final products are CO/CO_2, HCl/Cl_2 and H_2O. The data of S_{HCl} (selectivity to HCl) for all these catalysts is shown in Table 1. As listed in Table 1, all the catalysts represent high selectivity to the desired HCl (HCl is easier to be treated and less toxic than Cl_2), particularly for MO_y. Moreover, all the $(Ce,Cr)_xO_2/MO_y$ catalysts show more than 99% selectivity to CO_2, the carbon balance is (95–97)% while the chlorine balance is (89–94)%, implying that slight carbon and chlorine are deposited on the surface of the catalysts. Besides, the curves of the selectivity to HCl/CO_2 vs temperature over $(Ce,Cr)_xO_2$ and $(Ce,Cr)_xO_2/Nb_2O_5$ are provided in the Supplementary Material (see Fig. SM2). It can be seen from Fig. SM2 that two catalysts exhibit high selectivity to HCl/CO_2 in all the temperature ranges. It is worth noting that though HCl is the thermodynamically favored product at higher temperatures, Cl_2 can be formed through the Deacon reaction (1) in the presence of excess oxygen, thus, selectivity to HCl decreases slightly at higher temperatures.

$$2HCl(g) + 0.5O_2(g) \rightarrow H_2O(g) + Cl_2(g),$$

$$\triangle G_{298} = -38.0\,kJ\,mol^{-1}; \triangle H_{298} = -57.2\,kJ\,mol^{-1} \quad (1)$$

3.1.2. *Influence of oxygen concentration on the catalytic performance*

Fig. 2 shows the catalytic performances of the catalysts for DCE oxidation as a function of the oxygen concentration, in order to get more information for the oxidation process. It can be seen from Fig. 2(A) that within the range of 0–1% O_2, the values of TOF increase sharply as the increasing of the oxygen concentration. However, when the oxygen concentration exceeds 1% (four times of the value in theory for total oxidation of 1000 ppmv DCE), the values of TOF are almost unchanged. Moreover, it is worth noting that in the absence of oxygen, DCE conversion is still observed over these catalysts, which can be related to that the oxygen vacancies and acid sites on the catalyst surface participate in the destructive reaction. TOF value over Nb_2O_5 is smaller than that over $(Ce,Cr)_xO_2$, and TOF value over $(Ce,Cr)_xO_2/Nb_2O_5$ is the largest in the whole range, confirming the existence of synergistic effect between Nb_2O_5 and $(Ce,Cr)_xO_2$. Besides, as shown in Fig. 2(B) and (C), within the range of 0–1% O_2, the values of $T_{50\%}$ and $T_{90\%}$ decrease sharply as the increasing of the oxygen concentration. If the oxygen concentration exceeds 1%, these values decrease slightly. And in higher oxygen concentration, the values of $T_{50\%}$ and $T_{90\%}$ for $(Ce,Cr)_xO_2/Nb_2O_5$ are lower than other catalysts, further confirming the existence of synergistic effect between $(Ce,Cr)_xO_2$ and Nb_2O_5.

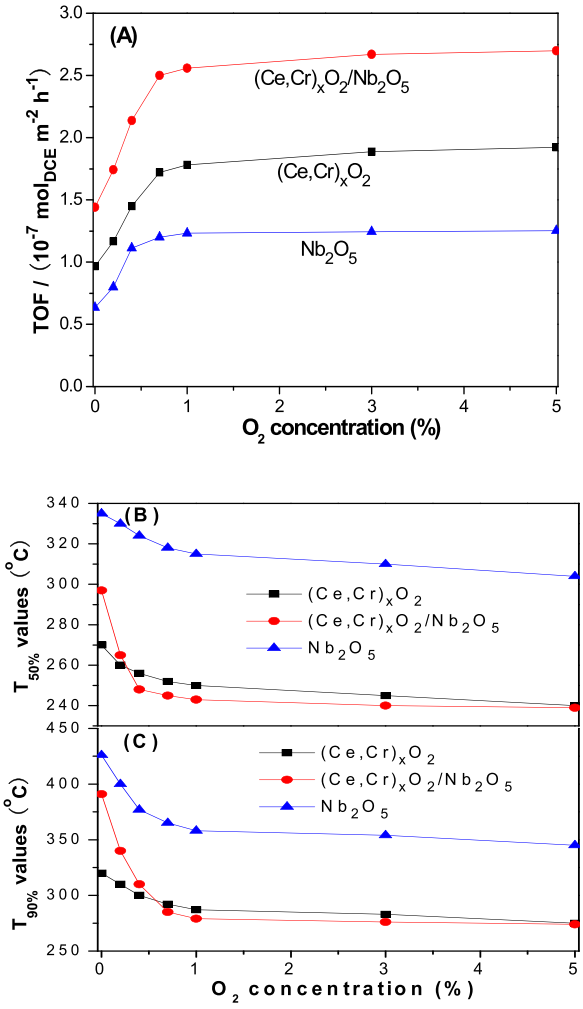

Fig. 2. Effect of O_2 concentration on the catalytic activities of $(Ce,Cr)_xO_2$, Nb_2O_5 and $(Ce,Cr)_xO_2/Nb_2O_5$: (A) TOF values (150 °C); (B) $T_{50\%}$ values and (C) $T_{90\%}$ values.

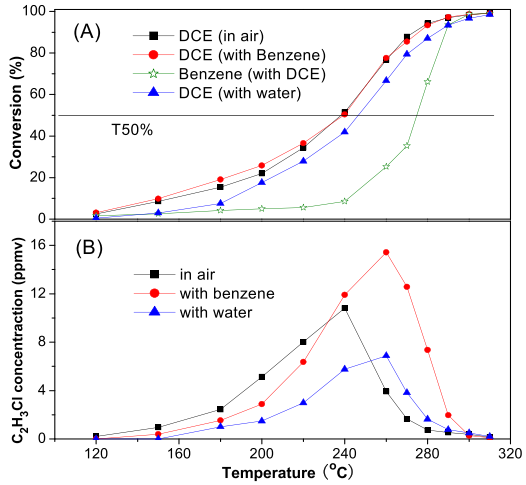

Fig. 3. Influence of water or benzene on the catalytic performances of $(Ce,Cr)_xO_2/Nb_2O_5$.

3.1.3. *Effect of water or benzene on the catalytic performance*

In practice, water and other VOCs always exist together with Cl-VOCs, and the presence of these components may have significant impact on the oxidative efficiency and the durability of the catalysts for Cl-VOCs elimination. As shown in Fig. 3(A), the

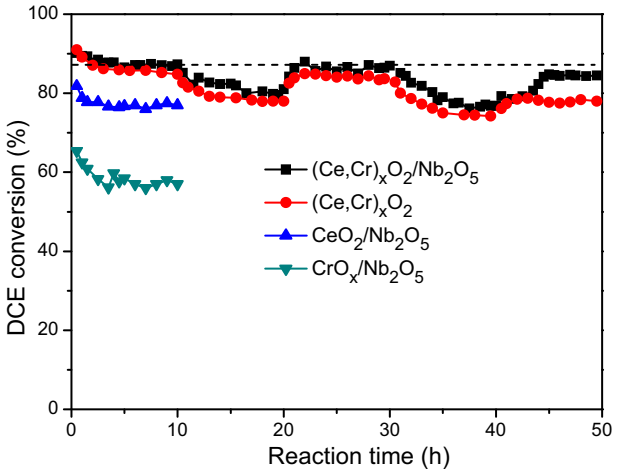

Fig. 4. Durability test for DCE oxidation over $(Ce,Cr)_xO_2/Nb_2O_5$, $(Ce,Cr)_xO_2$, CeO_2/Nb_2O_5 and CrO_x/Nb_2O_5 (265 °C).

value of $T_{50\%}$ for DCE oxidation over $(Ce,Cr)_xO_2/Nb_2O_5$ is increased slightly (8 °C) in the existence of 2.3% water, indicating that water inhibits DCE oxidation, because of its competitive adsorption on the active sites [4,18]. However, as shown in Fig. 3(B), less byproduct C_2H_3Cl is detected in the presence of water, which may be related to that water vapor promotes the removing of Cl species away from the catalyst surface in the form of HCl [4,20], thus, the —OH group on the catalyst surface can be recovered and it can promote the protonation of C_2H_3Cl, and then the protonated C_2H_3Cl can be further oxidized easily. Moreover, in the presence of benzene, benzene is more difficult to be oxidized than DCE at lower temperatures (below 290 °C), and the catalytic activity for DCE oxidation is almost unchanged with a little more C_2H_3Cl detected, which may be related to that benzene and DCE are adsorbed and oxidized on the different active sites of the catalyst, thus, the effect of competitive adsorption is not obvious [4]. Besides, this catalyst also shows high catalytic activity for benzene oxidation, since benzene can be totally destroyed below 300 °C in the existence of DCE.

The durability of the catalysts is investigated under different conditions and the results are shown in Fig. 4. As shown in Fig. 4, in the first 10 h under dry air condition, $(Ce,Cr)_xO_2$ shows high durability, though DCE conversion drops slightly in initial 2 h, because of the deposition of slight coke and Cl species on the catalyst surface [6,17]. When 2.3% water vapor is introduced, the catalytic activity of $(Ce,Cr)_xO_2$ decreases due to the competitive adsorption. Interestingly, if water is removed away from the reaction system, the activity can be completely recovered to the first stage. Moreover, when 1000 ppmv benzene is introduced in the fourth stage, DCE conversion decreases more obvious than the second stage, which can be related to the competitive adsorption/oxidation and the formation of more coke. However, if benzene is cut off, DCE conversion cannot be completely recovered, probably due to the coke formation in the fourth stage. As to $(Ce,Cr)_xO_2/Nb_2O_5$, the situation is similar, but the introduction of Nb_2O_5 and the strong metal-support interaction improve the catalytic activity and durability of $(Ce,Cr)_xO_2/Nb_2O_5$ for the resistance to water and benzene, making it promising to be applied in industry. For comparison, the durability tests of CeO_2/Nb_2O_5 and CrO_x/Nb_2O_5 are also conducted. As shown in Fig. 4, DCE conversion drops obviously in the initial stage over CeO_2/Nb_2O_5 and CrO_x/Nb_2O_5, and then it tends to be stable, but is obvious lower than $(Ce,Cr)_xO_2/Nb_2O_5$, indicating that the interaction between CeO_2 and CrO_x can improve the catalytic performance of $(Ce,Cr)_xO_2/Nb_2O_5$. Besides, it is worth noting that for used $(Ce,Cr)_xO_2$ and $(Ce,Cr)_xO_2/Nb_2O_5$, if regenerated in situ in dry air flow (75 mL min^{-1}) at 400 °C for 2 h, their catalytic activities can

be recovered completely, further indicating that the presence of coke and the surface chlorination are the reasons for the deactivation of the catalysts.

3.2. Catalyst characterization

3.2.1. XRD and UV-Raman characterization

The XRD patterns of the catalysts are displayed in Fig. 5(A) and (B). As shown in Fig. 5(A), the feature diffraction peaks of anatase TiO_2, V_2O_5, Nb_2O_5, MoO_3, WO_3 and La_2O_3 appear for the related MO_y support, respectively. From Fig. 5(B), it can seen that the characteristic diffraction peaks of CeO_2 with fluorite structure (at $2\theta = 28.6$, 33.0, 47.6 and 56.4°, respectively) [17,18] appear for $(Ce,Cr)_xO_2$, revealing the formation of cubic CeO_2 crystallites. While the feature diffraction peaks of Cr_2O_3 (at $2\theta = 33.6$, 36.3 and 54.9) [17,18] are rather weak, which can be related to that the Cr species is highly dispersed into the matrix of CeO_2. Chromium cannot combine with ceria to form Ce-Cr solid solution, due to the huge gap in the lattice parameters (the ionic radius of Ce^{4+} is 0.097 nm, much bigger than that of Cr^{3+} (0.052 nm)) and the limit of the Hume-Rothery rules. As to $(Ce,Cr)_xO_2/MO_y$, the feature diffraction peaks of CrO_x are not detected, indicating a high dispersion of Cr species into the matrix and/or the formation of Cr—M—O compounds. Especially, for $(Ce,Cr)_xO_2/MO_y$ (M = Ti, Nb and W), only the feature diffraction peaks of cubic CeO_2 and MO_y are observed. While for $(Ce,Cr)_xO_2/MO_y$ (M = V, Mo and La), the feature diffraction peaks of $CeVO_4$ [21], $CrVO_4$ [22] and V_2O_5 [21,23] are observed for $(Ce,Cr)_xO_2/V_2O_5$, CeO_2 and $Cr_{1.776}Mo_{0.112}O_3$ [24] for $(Ce,Cr)_xO_2/MoO_3$, and $Ce_{0.56}La_{0.44}O_{1.78}$ [25] for $(Ce,Cr)_xO_2/La_2O_3$, respectively. More details for $(Ce,Cr)_xO_2/MoO_3$ and $(Ce,Cr)_xO_2/La_2O_3$ are shown in Fig. SM3 in the Supplementary Material. The above results indicate that diverse crystal structure and composition are observed for the ternary metal oxides, which can affect the acid and redox properties of the catalysts and further influence their catalytic performances as further discussed below.

The Raman spectra of fluorite structure are sensitive to the crystalline symmetry and are related to the lattice oxygen vibrations. Fig. 5(C) and (D) show the UV-Raman spectra of the catalysts using a laser at 325 nm as the excitation source. As shown in Fig. 5(C), for MO_y supports, different feature peaks of TiO_2, V_2O_5, Nb_2O_5, MoO_3, WO_3 and La_2O_3 appear for each sample, respectively. As shown in Fig. 5(D), for $(Ce,Cr)_xO_2$ and $(Ce,Cr)_xO_2/MO_y$ (except for $(Ce,Cr)_xO_2/V_2O_5$), all the catalysts shows a strong peak at 450 cm^{-1}, which is connected with the F_{2g} Raman vibration mode of the cubic fluorite structure [18,26,27]. For $(Ce,Cr)_xO_2/V_2O_5$, this band with weaker intensity is assigned to the ν_2 mode of the VO_4^{3-} tetrahedra [21], and the feature peaks of $CeVO_4$ are observed obviously at 788 and 852 cm^{-1} [21], while the vibrational modes belonging to V_2O_5 [21,23] are rather weak. Moreover, no Raman signals assigned to Cr_2O_3 or CrO_3 are observed for these catalysts, because of the high dispersion and/or the formation of Cr—M—O compounds. The results mentioned above are agreed well with the results of XRD characterization.

Apart from the F_{2g}-related contribution, three new bands at ~325, 587 and 1166 cm^{-1} are also observed for all the samples (except for $(Ce,Cr)_xO_2/V_2O_5$). The bands at 587 and 1166 cm^{-1} can be assigned to the non-degenerate LO mode of CeO_2 due to the relaxation of symmetry rules, which is often connected with the oxygen vacancies in CeO_2 lattice [18]. The band at 325 cm^{-1} can be ascribed to the displacement of oxygen atoms from their ideal fluorite lattice positions [18], also implying the existence of defect structure. According to previous literatures [6,16], the oxygen vacancies favor the redox reaction and thus promote deep oxidation of Cl-VOCs over the catalysts. Since three peaks are overlapped by the Raman spectra of MO_y, the oxygen vacancies for these catalysts are further measured by XPS analysis shown below.

3.2.2. XPS characterization

The oxidation states and content of the elements on the catalyst surface are detected by XPS, and the results are shown in Fig. 6. It can be seen from Fig. 6(A) that eight peaks of Ce 3d spectra are detected for all the catalysts. Two peaks observed at v′ (centered at 883.8 eV) and u′ (centered at 901.9 eV) are the feature peaks of Ce^{3+}, while Ce^{4+} can be characterized by other six peaks [16,28,29]. The difference for the peak shapes of these catalysts can be related to the different ratios of Ce^{3+}/Ce^{4+}, generated from the strong interaction between Ce and other elements in the mixed oxides. It is notable that the existence of Ce^{3+} species indicates the oxygen vacancies in CeO_2, which is beneficial for promoting the mobility of active oxygen species [16,18]. As shown in Fig. 6(A) and (C), for $(Ce,Cr)_xO_2/MO_y$, though the Ce content for the bulk catalysts are the same, the Ce and Ce^{3+} content on the surface of the catalysts are different. The content of Ce^{3+} on the surface of these catalysts decreases in the order of $(Ce,Cr)_xO_2/V_2O_5 > (Ce,Cr)_xO_2 > (Ce,Cr)_xO_2/Nb_2O_5 > (Ce,Cr)_xO_2/TiO_2 > (Ce,Cr)_xO_2/WO_3 > (Ce,Cr)_xO_2/La_2O_3 > (Ce,Cr)_xO_2/MoO_3$, and this order is contrary to the order for the $T_{50\%}$ (except for $(Ce,Cr)_xO_2/La_2O_3$ and $(Ce,Cr)_xO_2/V_2O_5$), implying that the presence of Ce^{3+} species is favorable for improving the catalytic activities of the catalysts. However, for $(Ce,Cr)_xO_2/La_2O_3$ and $(Ce,Cr)_xO_2/V_2O_5$, their catalytic activities are poorer though more Ce^{3+} species exists, because of the formation of $CeVO_4$ and $Ce_{0.56}La_{0.44}O_{1.78}$, respectively, which has been confirmed by XRD and UV-Raman characterization.

Fig. 6(B) shows the Cr 2p spectra of the catalysts. The binding energies of Cr ($2p_{1/2}$) are 585.5 and 587.4 eV, associated with the Cr (III) and Cr (VI) in the mixed oxides, respectively. Cr ($2p_{3/2}$) binding energies, 576.2 and 578.6 eV, are related to the Cr (III) and Cr (VI), respectively [29,30]. The Cr^{6+} species result from the strong interaction of the chromium clusters with cerium oxide [16–18,29]. As shown in Fig. 6(B) and (C), the Cr and Cr^{6+} content on the surface of the catalysts are also quite different from each other. Similarly, the decreasing tendency of Cr^{6+} content is $(Ce,Cr)_xO_2 > (Ce,Cr)_xO_2/Nb_2O_5 > (Ce,Cr)_xO_2/TiO_2 > (Ce,Cr)_xO_2/WO_3 > (Ce,Cr)_xO_2/La_2O_3 > (Ce,Cr)_xO_2/MoO_3 > (Ce,Cr)_xO_2/V_2O_5$, and this order is contrary to the order for the $T_{50\%}$ (except for $(Ce,Cr)_xO_2/MoO_3$), indicating that the presence of Cr^{6+} species is favorable for improving the catalytic performances of the catalysts, due to its high oxidizing ability. For $(Ce,Cr)_xO_2/MoO_3$, the surface content of Cr^{6+} species is less because of the formation of $Cr_{1.776}Mo_{0.112}O_3$, confirmed by XRD and UV-Raman characterization.

3.2.3. SEM characterization

SEM photos of the catalysts are displayed in Fig. 7. As shown in Fig. 7(A), $(Ce,Cr)_xO_2$ exhibits rice-particle-like structure with smaller particle sizes. As to $(Ce,Cr)_xO_2/MO_y$ (M = Ti, Nb and W), it can be seen from Fig. 7(B), (D) and (F) that $(Ce,Cr)_xO_2$ is well dispersed on the matrix of the MO_y supports, though some agglomeration is observed. Particularly, much surface of Nb_2O_5 is exposed. Thus, the catalytic performances of these catalysts can be promoted because of the synergistic effect between $(Ce,Cr)_xO_2$ and MO_y. As to $(Ce,Cr)_xO_2/MO_y$ (M = V, Mo and La), it seems that the interface of $(Ce,Cr)_xO_2$ and MO_y is disappeared, implying the formation of Ce—M—O or Cr—M—O compounds. These results are in consistence with the characterization results of XRD and UV-Raman analysis.

3.2.4. NH_3-TPD characterization

The surface acid properties of the catalysts are characterized by NH_3-TPD measurement. The profiles are shown in Fig. 8 and

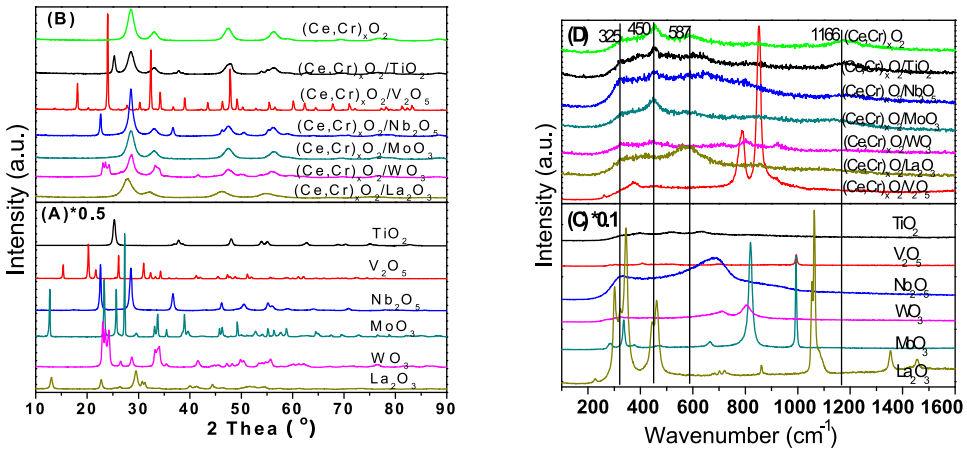

Fig. 5. XRD (A, B) and UV-Raman (C, D) patterns of the catalysts.

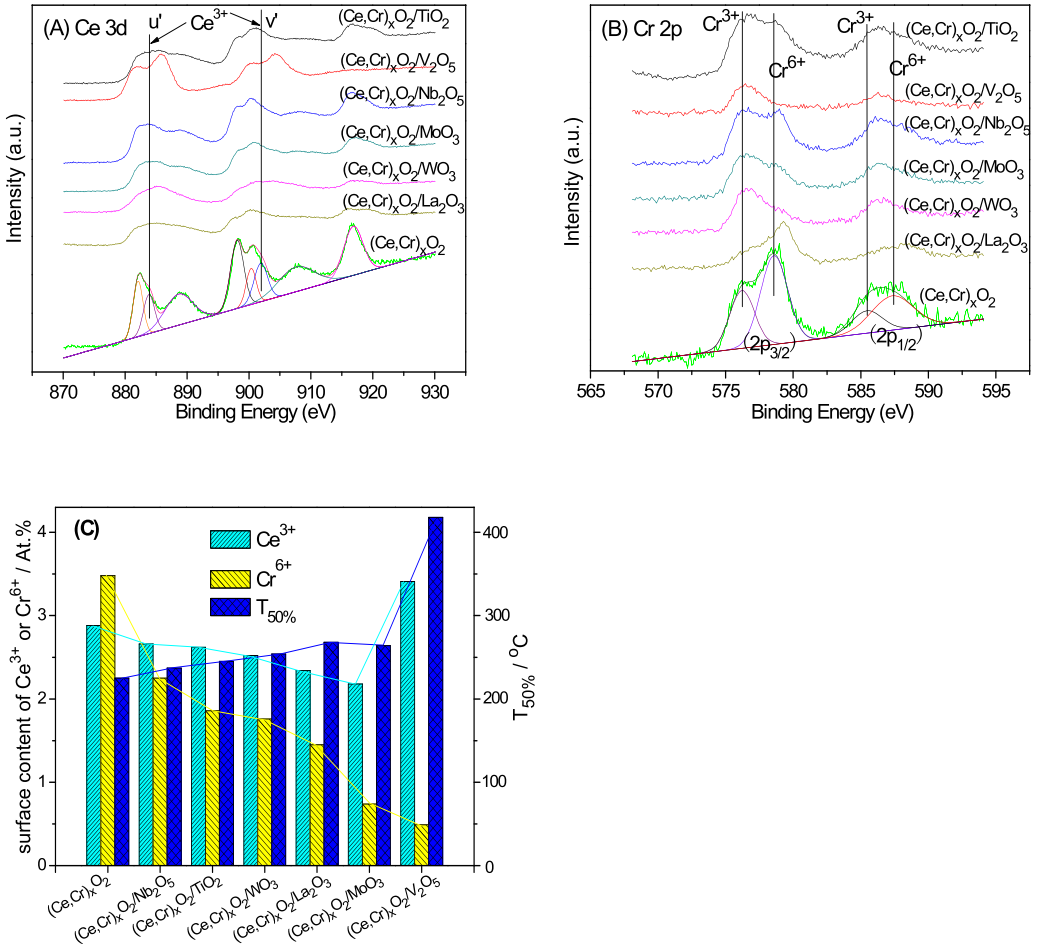

Fig. 6. XPS spectra of the catalysts: (A) Ce 3d, (B) Cr 2p and (C) relationship between values of TOF and ion content of Ce^{3+} or Cr^{6+} on the catalyst surface.

the related data is listed in Table 1. The peaks below 150 °C are considered as the desorption of the physical adsorbed NH_3. Two peaks are observed in the range of 150–450 °C. Peak α appears at lower temperatures is ascribed to weak acid sites (M^{n+}), while peak β is assigned to strong acid sites (—OH) [31,32]. For MO_y supports and $(Ce,Cr)_xO_2$, the desorption peaks of NH_3 for weak acid sites are all observed, particularly for V_2O_5, Nb_2O_5 and $(Ce,Cr)_xO_2$. While the desorption peaks of NH_3 for strong acid sites are only obvious for TiO_2, V_2O_5, Nb_2O_5 and $(Ce,Cr)_xO_2$, and they are rather weak for MoO_3, WO_3 and La_2O_3. It is noticeable that the acid concentration of TiO_2 is higher than Nb_2O_5, thus, the catalytic activity and the concentration of byproduct C_2H_3Cl for pure TiO_2 is higher than Nb_2O_5, since the acid sites are helpful for the dehydrochlorination of DCE to form the byproduct C_2H_3Cl. This is related to the nature of each metal oxide. For $(Ce,Cr)_xO_2/MO_y$ catalysts, the desorption peaks of NH_3 for both the weak and strong acid sites are observed, though they are rather weak for $(Ce,Cr)_xO_2/La_2O_3$. According to previous literatures [20,33], for Cl-VOCs oxidation, the strong acid sites are more important than the weak acid sites. As shown in Table 1, the concentration of the strong acid

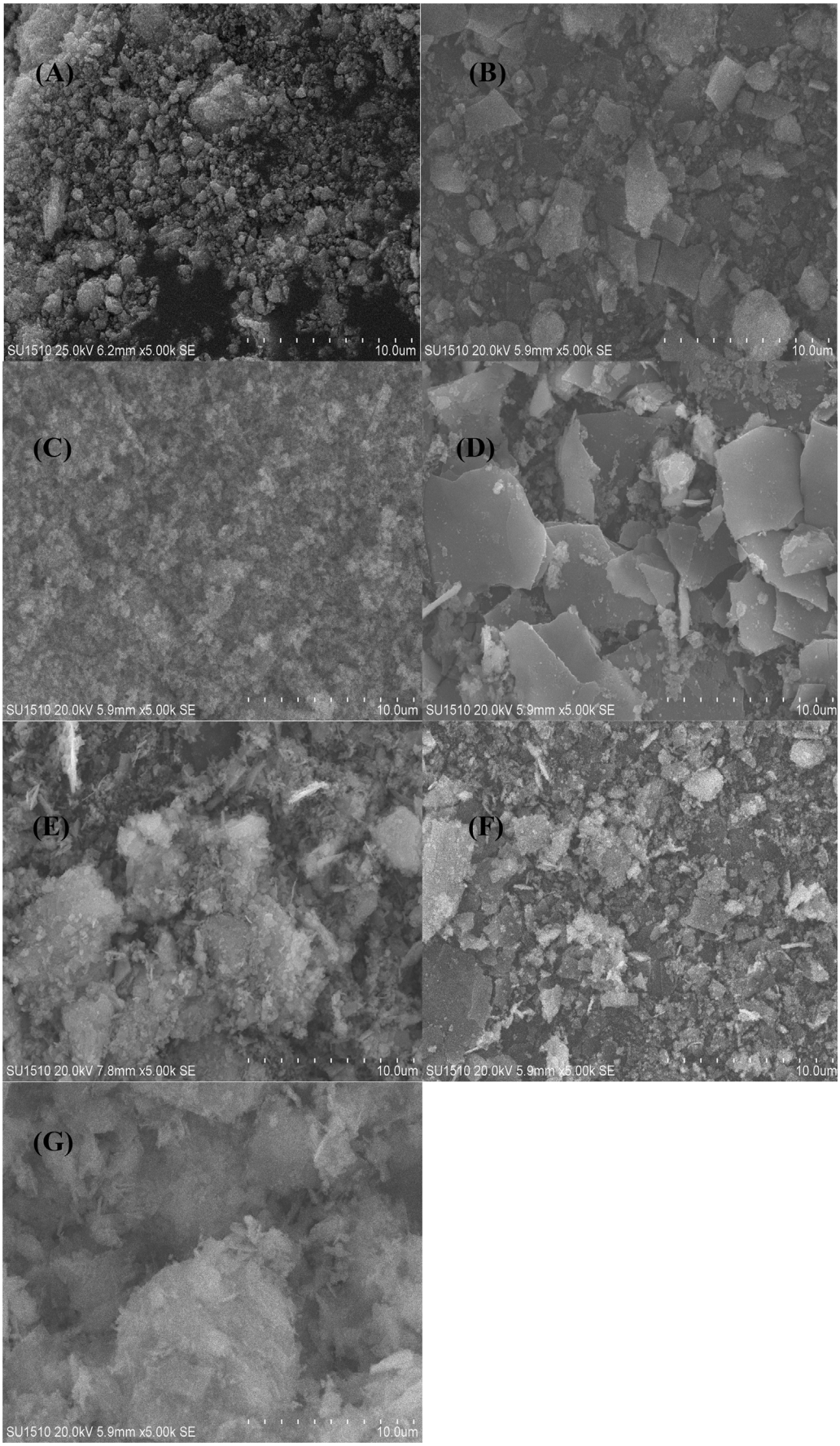

Fig. 7. SEM photos of the catalysts: (A) $(Ce,Cr)_xO_2$, (B) $(Ce,Cr)_xO_2/TiO_2$, (C) $(Ce,Cr)_xO_2/V_2O_5$, (D) $(Ce,Cr)_xO_2/Nb_2O_5$, (E) $(Ce,Cr)_xO_2/MoO_3$, (F) $(Ce,Cr)_xO_2/WO_3$ and (G) $(Ce,Cr)_xO_2/La_2O_3$.

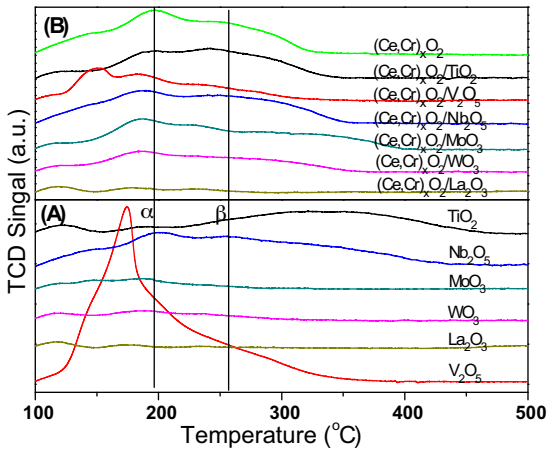

Fig. 8. NH_3-TPD curves of $(Ce,Cr)_xO_2$, MO_y and $(Ce,Cr)_xO_2/MO_y$ catalysts.

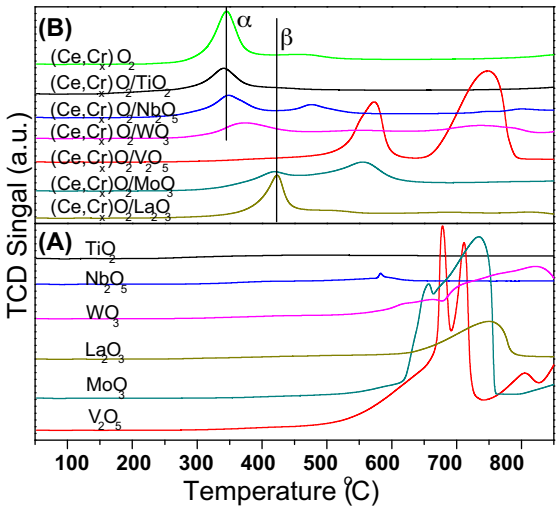

Fig. 9. H_2-TPR curves of $(Ce,Cr)_xO_2$, MO_y and $(Ce,Cr)_xO_2/MO_y$ catalysts.

sites on the surface of the catalysts decreases in the sequence of $(Ce,Cr)_xO_2/Nb_2O_5 \succ (Ce,Cr)_xO_2/TiO_2 \succ (Ce,Cr)_xO_2 \succ (Ce,Cr)_xO_2/MoO_3 \succ (Ce,Cr)_xO_2/V_2O_5 \succ (Ce,Cr)_xO_2/WO_3 \succ (Ce,Cr)_xO_2/La_2O_3$, and the concentration of the total acid sites is in the order of $(Ce,Cr)_xO_2/Nb_2O_5$, $(Ce,Cr)_xO_2/MoO_3 \succ (Ce,Cr)_xO_2 \succ (Ce,Cr)_xO_2/TiO_2 \succ (Ce,Cr)_xO_2/WO_3 \succ (Ce,Cr)_xO_2/V_2O_5 \succ (Ce,Cr)_xO_2/La_2O_3$, both of which are not consistent well with their inherent catalytic activities, indicating that the surface acid property is not the sole factor determining the catalytic performances of the catalysts.

3.2.5. H_2-TPR characterization

The redox properties of the catalysts are characterized by H_2-TPR measurement, and the results are shown in Fig. 9. As displayed in Fig. 9(A), for MO_y supports, the reduction peaks are rather weak below 600 °C, which are related to the reduction of surface and subsurface oxygen species, indicating that MO_y represent poor oxidizing ability at lower temperatures. The peaks above 600 °C are related to the reduction of MO_y and/or their intermediates produced in the reduction process [4,18,34]. Especially, the bulk oxygen in Nb_2O_5 and TiO_2 cannot be consumed below 850 °C. The diverse intensity and position of the reduction peaks are closely related to the nature of MO_y. For $(Ce,Cr)_xO_2$, as shown in Fig. 9(B), two H_2 consumption peaks are observed, and peak α (~354 °C) can be related to the reduction of Cr^{6+} to Cr^{3+} species [35–37], while peak β (~460 °C) is assigned to the reduction of the surface oxygen species on the catalyst surface [18]. The strong interaction between CeO_2 and CrO_x promotes the formation of Cr^{6+} species with high oxidizing ability (1.1 mmol H_2 g_{cat}^{-1}, account for 56% of the total Cr content, adopting known amount of CuO as the reference). For $(Ce,Cr)_xO_2/MO_y$ (M = Ti, Nb and W), peak α also appears with high signal intensity, which is favorable for deep oxidation of the organic reactants and the byproducts. As to $(Ce,Cr)_xO_2/MO_y$ (M = V, Mo and La), peak α is rather weak, and the reduction peaks for the bulk oxygen are obviously removed to much lower temperatures than MO_y, because of the formation of Ce—M—O and Cr—M—O compounds. The reducibility of these catalysts is in the sequence of $(Ce,Cr)_xO_2 \succ (Ce,Cr)_xO_2/Nb_2O_5 \succ (Ce,Cr)_xO_2/TiO_2 \succ (Ce,Cr)_xO_2/WO_3 \succ (Ce,Cr)_xO_2/MoO_3 \succ (Ce,Cr)_xO_2/La_2O_3 \succ (Ce,Cr)_xO_2/V_2O_5$, which is in agreement with their apparent catalytic activities (shown in Fig. 1), since the redox property of the catalyst is favorable for DCE destruction.

In all, from the results mentioned above, it can be seen that the synergy between the redox and acid property plays an important role for promoting the catalytic performances of the supported $(Ce,Cr)_xO_2$ catalysts for deep oxidation of DCE. This synergy is resulted from that the strong acid sites of the supports firstly promotes DCE adsorption and dehydrochlorination, while the strong oxidative sites of $(Ce,Cr)_xO_2$ is in favor of the deep oxidation of the reactant, the intermediates and byproducts as well as the reduction of coke and Cl accumulation on the catalyst surface. Especially, $(Ce,Cr)_xO_2/Nb_2O_5$ displays the best catalytic activity and good durability. Besides, compared to the HZSM-5 support [20], Nb_2O_5 exhibits weaker acid property and stronger redox property, and there also exists strong metal-support interaction for $(Ce,Cr)_xO_2/Nb_2O_5$. Thus, less byproduct C_2H_3Cl and less deactivation is observed for $(Ce,Cr)_xO_2/Nb_2O_5$ than $(Ce,Cr)_xO_2$/HZSM-5 that reported previously [20].

4. Conclusions

A series of $(Ce,Cr)_xO_2/MO_y$ mixed oxides (M = Ti, V, Nb, Mo, W and La, respectively) were synthesized by deposition-precipitation method, and then investigated for total oxidation of gaseous 1,2-dichloroethane, one of the typical chlorinated VOCs. The characterization results show that $(Ce,Cr)_xO_2$ mixed oxide is highly dispersed on the matrix of MO_y support (M = Ti, Nb and W), while Ce—M—O or Cr—M—O compounds are formed for $(Ce,Cr)_xO_2/MO_y$ (M = V, Mo and La). The nature of the MO_y support, the different crystal structure and the composition as well as the strong interaction between $(Ce,Cr)_xO_2$ and MO_y lead to the diverse acid/redox properties and surface elements distribution of the materials. The activity evaluation results show that these catalysts display diverse catalytic activities for DCE elimination, different selectivity to byproduct C_2H_3Cl and high selectivity to HCl and CO_2 (the desired final products). The enhanced catalytic performances of the catalysts can be connected with the improved redox properties and the increased content of Ce^{3+} and Cr^{6+} species on the catalyst surface. Among them, $(Ce,Cr)_xO_2/Nb_2O_5$ exhibits preferable catalytic performance. Moreover, the influence of water or benzene on DCE oxidation is also investigated and the results show that they slightly inhibit DCE conversion, because of the competitive adsorption for the active sites. As to the long-term continuous durability test, $(Ce,Cr)_xO_2/Nb_2O_5$ represents high durability under dry air condition, though slight deactivation is observed in the initial stage, because of the deposition of coke and Cl species on the catalyst surface. Though the presence of water or benzene inhibits DCE conversion, the catalytic activity can be recovered by the cut of water, while a little deactivation is found by the cut of benzene, since coke formed by benzene combustion has already been deposited

on the catalyst surface. The preferable catalytic activity, selectivity and durability indicate that $(Ce,Cr)_xO_2/Nb_2O_5$ deserves more attention and may be applied potentially in industry for the elimination of chlorinated organic pollutants.

Acknowledgement

The financial support from Nature Science Foundation of China (No. 21477109) is gratefully acknowledged.

Appendix A. Supplementary data

Supplementary data associated with this article can be found, in the online version, at http://dx.doi.org/10.1016/j.apcatb.2016.03.017.

References

[1] B.B. Huang, C. Lei, C.H. Wei, G.M. Zeng, Chlorinated volatile organic compounds (Cl-VOCs) in environment-sources potential human health impacts, and current remediation technologies, Environ. Int. 71 (2014) 118–138.
[2] T. Cai, H. Huang, W. Deng, Q.G. Dai, W. Liu, X.Y. Wang, Catalytic combustion of 1,2-dichlorobenzene at low temperature over Mn-modified Co_3O_4 catalysts, Appl. Catal. B 166–167 (2015) 393–405.
[3] M. Romero-Sáez, D. Divakar, A. Aranzabal, J.R. González-Velasco, J.A. González-Marcos, Catalytic oxidation of trichloroethylene over Fe-ZSM-5: influence of the preparation method on the iron species and the catalytic behavior, Appl. Catal. B 180 (2016) 210–218.
[4] Handbook of Heterogeneous Catalysis, in: G. Erlt, H. Knözinger, F. Schüth, J. Weitkamp (Eds.), Second ed., Wiley-VCH, Weinheim, 2008, pp. 2385–2411.
[5] S.F. Zuo, M.L. Ding, J. Tong, L.C. Feng, C.Z. Qi, Study on the preparation and characterization of a titanium-pillared clay-supported CrCe catalyst and its application to the degradation of a low concentration of chlorobenzene, Appl. Clay Sci. 105–106 (2015) 118–123.
[6] P. Yang, S.S. Yang, Z.N. Shi, F. Tao, X.L. Guo, R.X. Zhou, Accelerating effect of ZrO_2 doping on catalytic performance and thermal stability of CeO_2–CrO_x mixed oxide for 1,2-dichloroethane elimination, Chem. Eng. J. 285 (2016) 544–553.
[7] S. Ojala, S. Pitkäaho, T. Laitinen, N.N. Koivikko, R. Brahmi, J. Gaálová, L. Matejova, A. Kucherov, S. Päivärinta, C. Hirschmann, T. Nevanperä, M. Riihimäki, M. Pirilä, R.L. Keiski, Catalysis in VOC abatement, Top. Catal. 54 (2011) 1224–1256.
[8] A. Aranzabal, B. Pereda-Ayo, M.P. González-Marcos, J.A. González-Marcos, R. López-Fonseca, J.R. González-Velasco, State of the art in catalytic oxidation of chlorinated volatile organic compounds, Chem. Pap. 68 (2014) 1169–1186.
[9] P. Yang, X.M. Xue, Z.H. Meng, R.X. Zhou, Enhanced catalytic activity and stability of Ce doping on Cr supported HZSM-5 catalysts for deep oxidation of chlorinated volatile organic compounds, Chem. Eng. J. 234 (2013) 203–210.
[10] L. Intriago, E. Díaz, S. Ordóñez, A. Vega, Combustion of trichloroethylene and dichloromethane over protonic zeolites: influence of adsorption properties on the catalytic performance, Microporous Mesoporous Mater. 91 (2006) 161–169.
[11] S. Chatterjee, H.L. Greene, Y.J. Park, Deactivation of metal exchanged zeolite catalysts during exposure to chlorinated hydrocarbons under oxidizing conditions, Catal. Today 11 (1992) 569–596.
[12] S. Maghsoodi, J. Towfighi, A. Khodadadi, Y. Mortazavi, The effects of excess manganese in nano-size lanthanum manganite perovskite on enhancement of trichloroethylene oxidation activity, Chem. Eng. J. 215-216 (2013) 827–837.
[13] X.Y. Wang, Q. Kang, D. Li, Catalytic combustion of chlorobenzene over MnO_x–CeO_2 mixed oxide catalysts, Appl. Catal. B 86 (2009) 166–175.
[14] B. de Rivas, R. López-Fonseca, M.A.í Gutiérrez-Ortiz, J.I. Gutiérrez-Ortiz, Structural characterisation of $Ce_{0.5}Zr_{0.5}O_2$ modified by redox treatments and evaluation for chlorinated VOC oxidation, Appl. Catal. B 101 (2011) 317–325.
[15] B. de Rivas, N. Guillén-Hurtado, R. López-Fonseca, F. Coloma-Pascual, A. García-García, J.I. Gutiérrez-Ortiz, A. Bueno-López, Activity selectivity and stability of praseodymium-doped CeO_2 for chlorinated VOCs catalytic combustion, Appl. Catal. B 121–122 (2012) 162–170.
[16] P. Yang, Z.H. Meng, S.S. Yang, Z.N. Shi, R.X. Zhou, Highly active behaviors of CeO_2–CrO_x mixed oxide catalysts in deep oxidation of 1,2-dichloroethane, J. Mol. Catal. A 393 (2014) 75–83.
[17] P. Yang, Z.N. Shi, S.S. Yang, R.X. Zhou, High catalytic performances of CeO_2–CrO_x catalysts for chlorinated VOCs elimination, Chem. Eng. Sci. 126 (2015) 361–369.
[18] P. Yang, S.S. Yang, Z.N. Shi, Z.H. Meng, R.X. Zhou, Deep oxidation of chlorinated VOCs over CeO_2-based transition metal mixed oxide catalysts, Appl. Catal. B 162 (2015) 227–235.
[19] Z.H. Meng, P. Yang, R.X. Zhou, Influence of Ce/Cr ratio on CeO_2–CrO_x mixed oxide catalysts for the catalytic oxidation of 1 2-dichloroethane, Acta Phys.-Chim. Sin. 29 (2013) 391–396.
[20] P. Yang, Z.N. Shi, F. Tao, S.S. Yang, R.X. Zhou, Synergistic performance between oxidizability and acidity/texture properties for 1,2-dichloroethane oxidation over $(Ce,Cr)_xO_2$/zeolite catalysts, Chem. Eng. Sci. 134 (2015) 340–347.
[21] U.O. Krašovec, B. Orel, A. Šurca, N. Bukovec, R. Reisfeld, Structural and spectroelectrochemical investigations of tetragonal $CeVO_4$ and Ce/V-oxide sol-gel derived ion-storage films, Solid State Ionics 118 (1999) 195–214.
[22] T. Tojo, Q.W. Zhang, F. Saito, Mechanochemical synthesis of rutile-type $CrMO_4$ (M = V, Sb) and their solid solutions, J. Solid State Chem. 179 (2006) 433–437.
[23] H. Huang, Y.F. Gu, J. Zhao, X.Y. Wang, Catalytic combustion of chlorobenzene over VO_x/CeO_2 catalysts, J. Catal. 326 (2015) 54–68.
[24] S.N. Liu, Z.D. Liu, Y.T. Wang, J. Tang, A comparative study on the high temperature corrosion of TP347H stainless steel, C22 alloy and laser-cladding C22 coating in molten chloride salts, Corros. Sci. 83 (2014) 396–408.
[25] B. Zhang, D. Li, X.Y. Wang, Catalytic performance of La-Ce-O mixed oxide for combustion of methane, Catal. Today 158 (2010) 348–353.
[26] T. Taniguchi, T. Watanabe, N. Sugiyama, A.K. Subramani, H. Wagata, N. Matsushita, M. Yoshimura, Identifying defects in ceria-based nanocrystals by UV Resonance Raman spectroscopy, J. Phys. Chem. C 113 (2009) 19789–19793.
[27] R. Si, Y.W. Zhang, S.J. Li, B.X. Lin, C.H. Yan, Urea-based hydrothermally derived homogeneous nanostructured $Ce_{1-x}Zr_xO_2$ (x = 0-0.8) solid solutions: a strong correlation between oxygen storage capacity and lattice strain, J. Phys. Chem. B 108 (2004) 12481–12488.
[28] R.Y. Qu, X. Gao, K.F. Cen, J.H. Li, Relationship between structure and performance of a novel cerium-niobium binary oxide catalyst for selective catalytic reduction of NO with NH_3, Appl. Catal. B 142–143 (2013) 290–297.
[29] P. Singh, M.S. Hegde, J. Gopalakrishnan, $Ce_{2/3}Cr_{1/3}O_{2+y}$: a new oxygen storage material based on the fluorite structure, Chem. Mater. 20 (2008) 7268–7273.
[30] S.D. Yim, I.-S. Nam, Characteristics of chromium oxides supported on TiO_2 and Al_2O_3 for the decomposition of perchloroethylene, J. Catal. 221 (2004) 601–611.
[31] A. Corma, H. García, Lewis acids as catalysts in oxidation reactions: from homogeneous to heterogeneous systems, Chem. Rev. 102 (2002) 3837–3892.
[32] M.A. Bañares, I.E. Wachs, Molecular structures of supported metal oxide catalysts under different environments, J. Raman Spectrosc. 33 (2002) 359–380.
[33] J.R. González-Velasco, R. López-Fonseca, A. Aranzabal, J.I. Gutiérrez-Ortiz, P. Steltenpohl, Evaluation of H-type zeolites in the destructive oxidation of chlorinated volatile organic compounds, Appl. Catal. B 24 (2000) 233–242.
[34] F. Bertinchamps, C. Grégoire, E.M. Gaigneaux, Systematic investigation of supported transition metal oxide based formulations for the catalytic oxidative elimination of (chloro)-aromatics, Part I: identification of the optimal main active phases and supports, Appl. Catal. B 66 (2006) 1–9.
[35] J.Y. Luo, M. Meng, J.S. Yao, X.G. Li, Y.Q. Zha, X.T. Wang, T.Y. Zhang, Preparation and characterization of magnesia-supported chromium catalysts for the fluorination of 1,1,1-trifluoro-2-chloroethane (HCFC-133a), Appl. Catal. B 87 (2009) 92–103.
[36] S.D. Yim, K.H. Chang, I.-S. Nam, Deactivation of chromium oxide catalyst for the removal of perchloroethylene (PCE), Stud. Surf. Sci. Catal. 139 (2001) 173–180.
[37] S.D. Yim, D.J. Koh, I.-S. Nam, Y.G. Kim, Effect of the catalyst supports on the removal of perchloroethylene (PCE) over chromium oxide catalysts, Catal. Lett. 64 (2000) 201–207.